Strategic Approach to Pyrazinoquinoxaline Molecular Design for Enhanced Performance.

Sunil Madagyal,[a] Pratima Yadav, [a] Prabhakar Chetti,[b] Atul Chaskar [a*]

[a]Department of Chemistry, Institute of Chemical Technology, Mumbai, N.P.Marg., Matunga, Mumbai-400019, Maharashtra, India.

[b]Department of Chemistry, National Institute of Technology, Kurukshetra.

*Corresponding author: ac.chaskar@ictmumbai.edu.in (AC)

Abstract –

The availability of affordable organic compounds with thermally activated delayed fluorescence (TADF) properties represents a unique class of materials for addressing key challenges in organic electronics. In this context, we have successfully designed and synthesised three novel hybrid molecules 2-(4-(3,6-di-tert-butyl-9H-carbazol-9-yl)phenyl)-3,7,8-triphenylpyrazino[2,3-g]quinoxaline **(*t*Cz-PyrQx),** 4-(tert-butyl)-N-(4-(tert-butyl)phenyl)-N-(4-(3,7,8-triphenylpyrazino[2,3-g]quinoxalin-2-yl)phenyl)aniline **(*t*DPA-PyrQx)**, and 2-(4-(9,9-dimethylacridin-10(9H)-yl)phenyl)-3,7,8-triphenylpyrazino[2,3-g]quinoxaline **(Ac-PyrQx)** comprising electron-donating 3,6-di-*tert*-butyl-9H-carbazole, bis(4-(tert-butyl)phenyl)amine, and (9,9-dimethyl-9,10-dihydroacridine) with electron-accepting pyrazinoquinoxaline groups. The incorporation of highly planar and rigid pyrazinoquinoxaline electron-accepting moieties holds significant importance due to their unique properties like efficient charge transfer, and reduced steric hindrance. Their planar structure facilitates strong π-π stacking interactions and efficient charge transfer within the molecular framework, leading to improved exciton formation and enhanced reverse intersystem crossing (RISC) rates, which are critical for TADF processes. The three different electron-donating groups with pyrazinoquinoxaline were synthesised with the view of tuning the photophysical and electrochemical properties of the hybrids.

Key Words – Pyrazinoquinoxaline, π-π stacking interactions, reverse intersystem crossing (RISC), red TADF, OLED.

Introduction –

In the past decade, a family of luminescent materials referred to as thermally activated delayed fluorescence (TADF) have attracted great attention as an alternative for noble metal-based phosphorescent materials in organic light-emitting diodes (OLEDs). Advancements in materials design, synthesis, and device engineering continue to push the boundaries of OLED technology, bringing us closer to achieving efficient red TADF for practical applications in displays and lighting.[1–6] Due to their advantages of 100% internal quantum efficiency via the reverse intersystem crossing (RISC) process from the triplet (T_1) state to the singlet (S_1) state, pure organic thermally activated delayed fluorescence (TADF) emitters have attracted a lot of attention for applications in organic light-emitting diodes (OLEDs).[7–9] Because TADF-based OLEDs have outstanding characteristics, including high external quantum efficiencies (EQEs)[10–12], high light brightness and stability[13], and high color purity[14,15]. The efficiency of TADF emitters is notably enhanced as approximately 75% of spin-forbidden triplet excitons can transition from the singlet state to the ground state through an up-conversion process. Some purely organic TADF material exhibit 100% internal quantum efficiencies (IQEs).[16–19] The breakthroughs in molecular design and materials engineering within the TADF field not only expand the color possibilities of emitters but also significantly boost their efficiency. These advancements promise a future where TADF-based OLEDs play a central role in shaping energy-efficient, visually stunning displays, and lighting systems controlled spatial overlap between Highest Occupied Molecular Orbital (HOMO) and Lowest Unoccupied Molecular Orbital (LUMO) is crucial for achieving a high photoluminescence quantum yield (PLQY). Additionally, introducing a twist between HOMO and LUMO reduces the singlet-triplet energy gap.[20] These factors are pivotal in enhancing the (EQE) of OLEDs. Specifically, raising the optical outcoupling efficiency of OLEDs further augments the EQE, contributing to the overall improvement of OLED performance.[21–25]

To attain emission in red region, TADF molecules requires a substantial conjugated system, effectively reducing the energy gap between the lowest singlet excited state and lowest triplet excited state. To achieve this, electron-accepting moieties with potential electron-withdrawing effects and fused ring structure are favored. Commonly used acceptors for red emission includes pyrazino-2,3-dicabonitrile[26], 2,3-dicyanopyrazino phenanthroline[27], phenazine[28–31], quinaxolines[32–34], acenaphtho-pyrazine[35,36] and acenaphtho[1,2-b]quinoxaline[37] and electron donors as aromatic amines like carbazole, diphenylamine, phenoxazine, phenothiazine, dimethyl acridine are used in TADF molecules. These donors possess strong electron-donating capabilities

and stable, high-energy triplet states. Recently, pyrazinoquinoxaline is used as new acceptor unit because of its highly extended π-conjugation and the presence of structural elements that enhance its rigidity. Jain Pei and co-workers developed tetra substituted pyrazino[2,3-g]quinoxaline derivatives with thiophen and phenyl rings, which leads to changing extent of conjugation to achieve high efficiency active wavelength fibers.[38] Habin Su and co-workers developed pyrazino[2,3-g]quinoxaline derivatives with effect of substitution on different position and it was shown that combination of conjugation and cross conjugation effects is responsible for electronic properties.[39,40] Levent Toppare and co-workers have synthesized molecule having pyrazino[2,3-g]quinoxaline moiety demonstrate 84% optical contract in NIR with higher stability.[41] Yuxia Zhao and co-workers synthesized a water soluble pyrazino[2,3-g]quinoxaline based photosensitizer which exhibit both high fluorescence quantum yield and singlet oxygen quantum yield.[42] Achalkumar Sudhakar and coworkers developed material for bright green organic light emitting diodes that displaces an EQE 5% and they also developed solution processable pyrazino[2,3-g]quinoxaline Carbazole derivative to achieve 15.3% EQE for yellowish-green OLED and 12% EQE for white OLED.[43,44]

Herein, for the further π-extended and more rigidified acceptor units for TADF emitters, we have introduced 2,3,7,8-tetraphenylpyrazino[2,3-g]quinoxaline (pyrazinoquinoxaline) as an acceptor unit where the acceptor strength of the quinoxaline unit was further increased by fusing one extra pyrazino unit. This rigid pyrazinoquinoxaline acceptor unit was attached to the 9,9-dimethyl-9,10-dihydroacridine (Ac), bis(4-(tert-butyl)phenyl)amine (tDPA) and 3,6-di-tert-butyl-9H-carbazole (*t*Cz) donor units through phenyl ring spacer to enable sufficient twist between the donor and acceptor unit. Photophysical study of the three emitters, 2-(4-(3,6-di-tert-butyl-9H-carbazol-9-yl)phenyl)-3,7,8-triphenylpyrazino[2,3-g]quinoxaline (*t*Cz-PyrQx), 4-(tert-butyl)-N-(4-(tert-butyl)phenyl)-N-(4-(3,7,8-triphenylpyrazino[2,3-g]quinoxalin-2-yl)phenyl)aniline (*t*DPA-PyrQx), and 2-(4-(9,9-dimethylacridin-10(9H)-yl)phenyl)-3,7,8-triphenylpyrazino[2,3-g]quinoxaline (Ac-PyrQx) was performed in different organic solvent.

Results and Discussion –

Molecular Design Strategy

The design and synthesis of TADF materials have been modified recently, with a focus on enhancing their performance properties across various spectral ranges. This involves manipulating

the molecular structure by introducing specific acceptor and donor units, spacers, and linkers to optimize the electronic properties, energy levels, and exciton dynamics for improved OLED device performance.

Recently, it was shown that extending the conjugation length and optimizing the electron-accepting potential of acceptor moieties enhance the device performance of orange-red to deep-red TADF materials.[45–51]

In this work, we introduced pyrazinoquinoxaline as a acceptor unit because of its highly extended π-conjugation and the presence of structural elements that enhance its rigidity. Further, to enable proper twists between the donor and acceptor units, we added a phenyl ring spacer in between them. The introduction of the strong acceptor pyrazinoquinoxaline as a new acceptor unit was further increased by attaching the peripheral phenyl ring decorated extra pyrazino unit character of the pyrazinoquinoxaline unit, which control the electron-accepting characters and molecular orbitals of the acceptor moieties. The D-π-A primary skeleton was selected for its strong oscillator strength. The choice of donor can significantly influence the molecule's electronic properties and energy levels. To change the emission wavelength, the donors 9,9-dimethyl-9,10-dihydroacridine, bis(4-(tert-butyl)phenyl)amine, and 3,6-di-tert-butyl-9H-carbazole were used. The 9,9-dimethylacridine donor was the strong donor for orange emission, whereas bis(4-(tert-butyl)phenyl)amine and *t*-butyl carbazole donor was the weak donor for yellow emission. The combination of three donors with one acceptor produces three TADF emitters, namely ***t*Cz-PyrQx**, ***t*DPA-PyrQx** and **Ac-PyrQx**. **Scheme 1** shows the chemical structures of the TADF emitters.

Synthesis -

Scheme 1 represents the synthetic pathway that we followed to prepare ***t*CzPyrQx, *t*DPA-PyrQx,** and **Ac-PyrQx** along with intermediate. Crucial intermediate 2, 3-diphenylquinoxaline-6,7-diamine (I) obtained by condensation of 1,2,4,5-benzene tetramine tetrahydrochloride and benzyl which was further condensed with 1-(4-(3,6-di-tert-butyl-9H-carbazol-9-yl)phenyl)-2-phenylethane-1,2-dione, 1-(4-(bis(4-(tert-butyl)phenyl)amino)phenyl)-2-phenylethane-1,2-dione, and 1-(4-(9,9-dimethylacridin-10(9H)-yl)phenyl)-2-phenylethane-1,2-dione to get the compounds.

All the products were purified by column chromatography. The chemical structures of all these synthesized molecules are confirmed by ^{1}H NMR, ^{13}C NMR, and mass analysis.

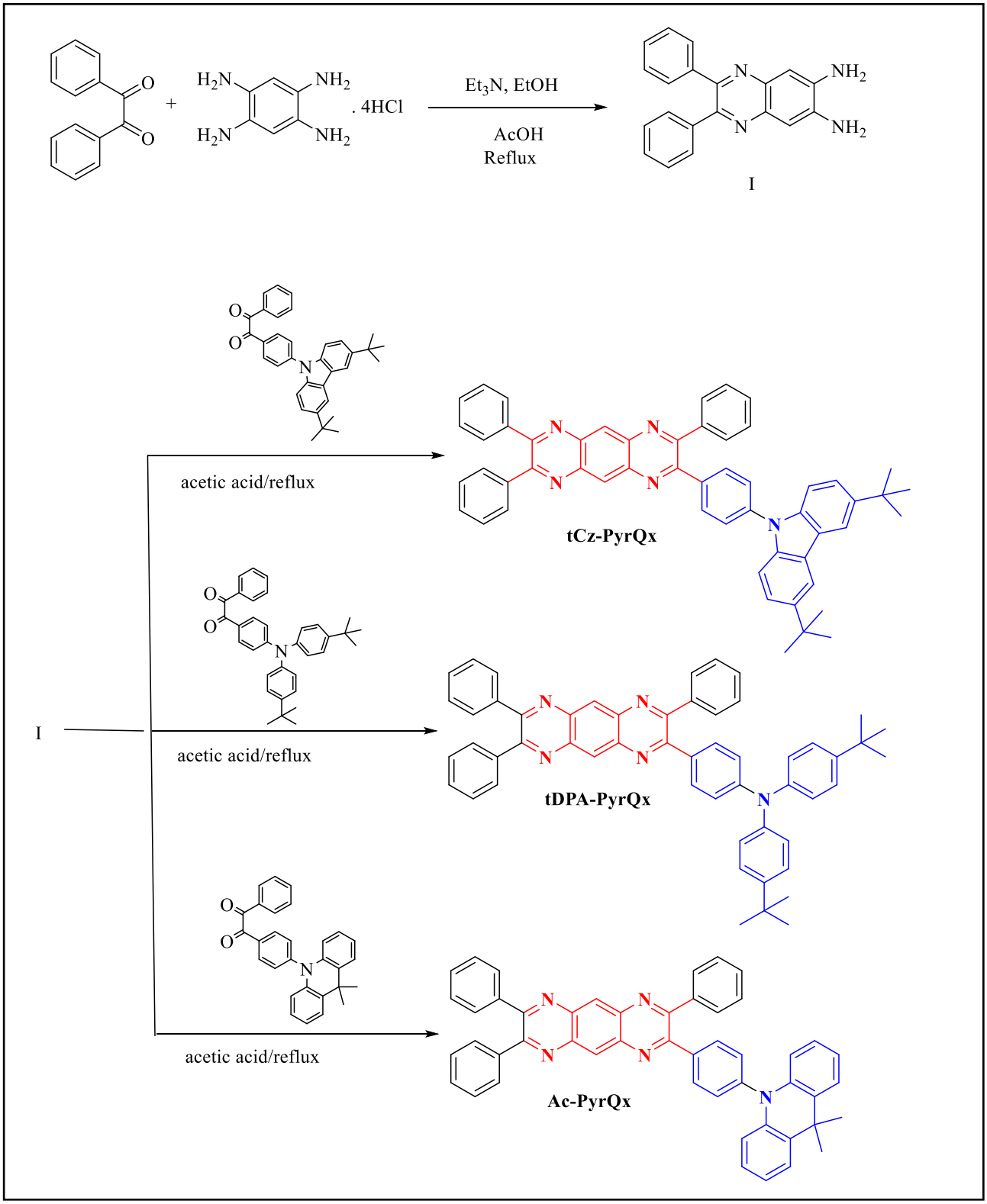

Scheme 1 Synthetic route of three TADF emitters**, *t*Cz-PyrQx**, ***t*DPA-PyrQx,** and **Ac-PyrQx,** and their chemical structures.

Photophysical Properties –

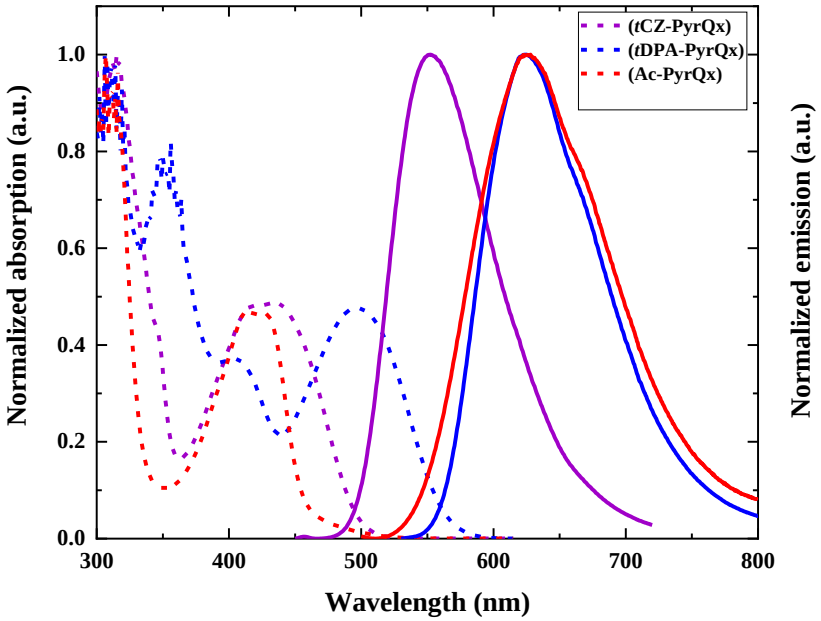

Fig. 1 Photophysical properties of TADF emitter's *t*Cz-PyrQx, *t*DPA-PyrQx and Ac-PyrQx

To evaluate the donor effect on PyrQx acceptor, the photophysical properties of the three compounds were studied using ultraviolet-visible (UV-Vis) and a fluorescence spectrometer in toluene (10^{-5} M) (**Fig. 1**) The strong absorption band observed at 316, 306, and 315 nm in toluene respectively, which are attributed to π-π* transitions. In addition, there are low-energy broad weak absorption peaks (400-500 nm) which are associated with the intramolecular charge transfer (ICT) states between Pyrazinophenazine acceptor and different donors used. It can be observed that the ICT-based absorption peak wavelengths of all three TADF-emitters are broadly varied from 400 nm to 520 nm depending on the strength of the differently substituted donor units. Interestingly, the ICT absorption bands gradually red-shifted from 422 nm **(*t*Cz-PyrQx)** to 496 nm **(*t*DPA-PyrQx)** with the increase of the electron-donating ability from *t*Cz to *t*DPA and the same trend is reflected in their respective PL spectra. The fluorescence emission peaks of ***t*Cz-PyrQx, *t*DPA-PyrQx**, and **Ac-PyrQx** are 552, 625 and 626 nm in toluene respectively. Broad and red-shifted emission spectrum of Carbazole substituted ***t*Cz-PyrQx** show slightly red-shifted emission and

diphenyl amine substituted ***t*DPA-PyrQx** and acridine substituted **Ac-PyrQx** suggests a very strong ICT characteristic of this compound. The emission spectrum all emitters (**Fig. 2**) exhibited very strong solvatochromism (180 nm) from non-polar cyclohexane to polar chloroform solvent indicating the presence of strong CT characteristics.

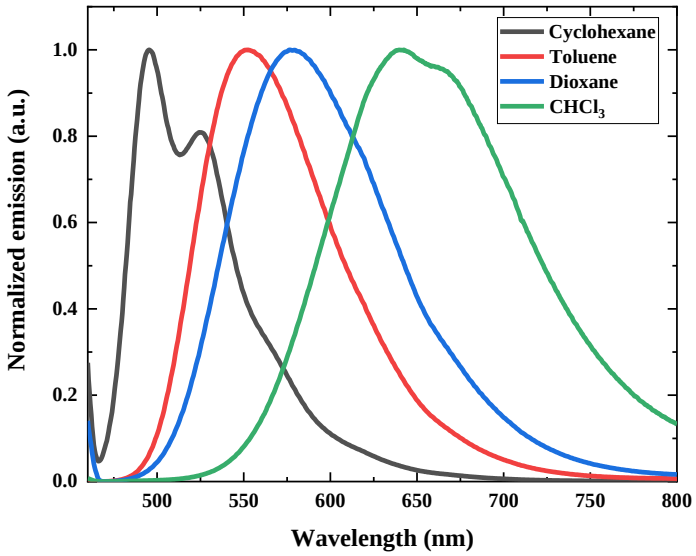

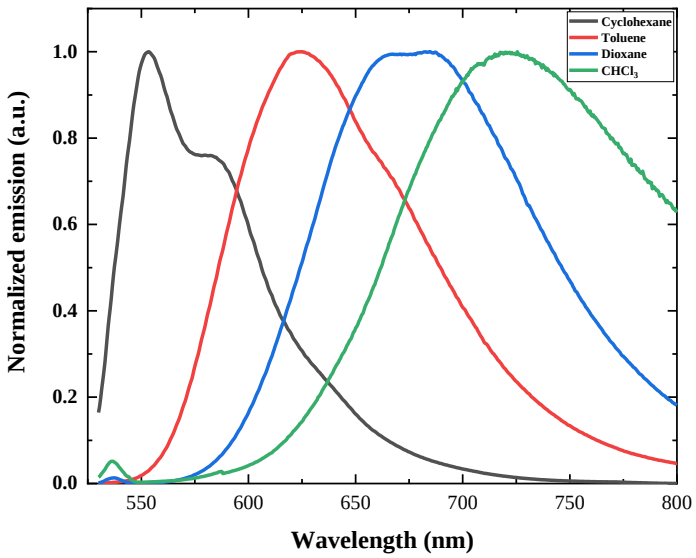

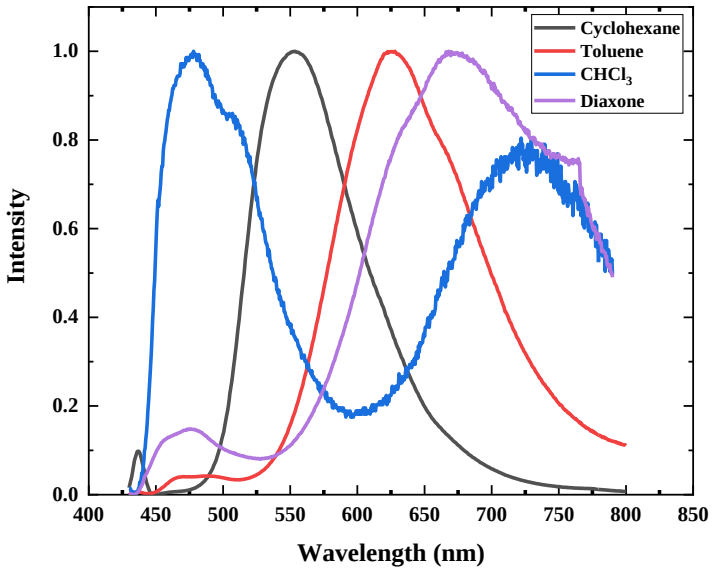

Fig. 2 PL spectra of ***t*Cz-PyrQx, *t*DPA-PyrQx** and **Ac-PyrQx** in different organic solvents at room temperature.

Thermal Properties –

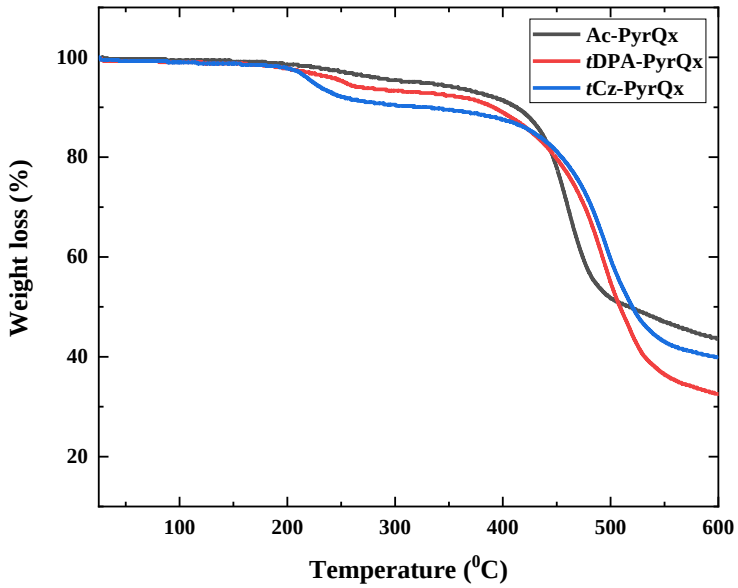

Fig. 3 Thermal gravimetric analysis (TGA) curves of ***t*Cz-PyrQx**, ***t*DPA-PyrQx**, and **Ac-PyrQx** emitters.

The thermal properties of these three TADF molecules is studied by Thermogravimetric analysis under nitrogen atmosphere. These molecules shows high thermal decomposition temperature at 236^0C, 337^0C and 350^0C respectively shown in **(Fig. 3)**. The high glass transition and decomposition temperatures implies higher thermal stability due to the high molecular weight and presence of strong pyrazinoquinoxaline acceptor with four nitrogen atoms in their moieties. Albeit, the extended conjugation leads to high morphological stability in the film.

Electrochemical Properties –

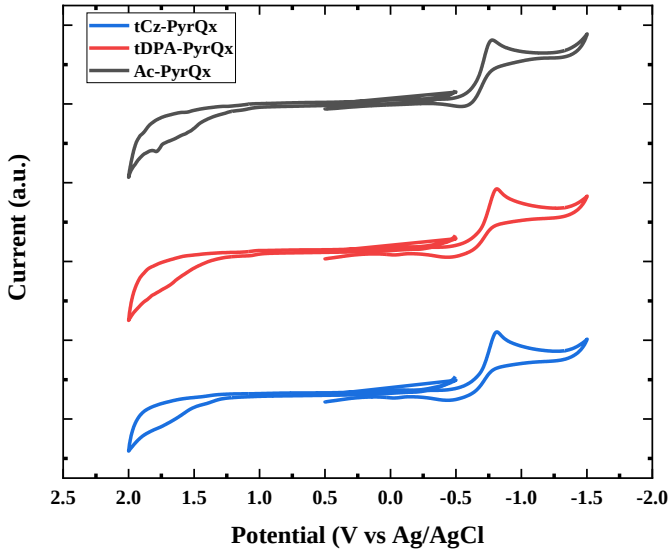

Fig. 4 Cyclic voltammogram of ***t*Cz-PyrQx**, ***t*DPA-PyrQx,** and **Ac-PyrQx** 0.1 M TBAP (reduction) in DMF and 0.1 M $TBAPF_6$ (oxidation) in CH_2Cl_2 were used as supporting electrolytes. A glassy carbon electrode was used as the working electrode; scan rate: 100 mV s^{-1}.

We used cyclic voltammetry (CV) to probe the electrochemical properties of the three emitter's ***t*Cz-PyrQx**, ***t*DPA-PyrQx,** and **Ac-PyrQx (Fig. 4).** A standard 3-electrode cell comprising silver/silver chloride (Ag/AgCl), a platinum wire, and a glassy carbon electrode as the reference, counter, and working electrodes, respectively were used. Tetrabutylammonium hexafluorophosphate ($TBAPF_6$ 0.1M) in DCM and tetrabutylammonium perchlorate (TBAP, 0.1M) in DMF were used as the supporting electrolyte for oxidation and reduction scan,

respectively. The energies of the HOMO levels were determined from the first oxidation potentials by taking the known E_{HOMO} of ferrocene (Fc) (−4.80 eV) as the reference value. The E_{ox} of Fc/ ferrocenium (Fc+) versus Ag/Ag^{+} as internal standard was measured to be −0.44 V and E_{HOMO} values of all measured compounds were calculated according to the equation: E_{HOMO} [eV] = −[E_{ox} − 0.44] − 4.80 and E_{LUMO} = E_{HOMO} + E_g. ***t*Cz-PyrQx, *t*DPA-PyrQx, and Ac-PyrQx** exhibit reversible redox processes with initial oxidation potentials of 1.68, 1.70 and 1.78 eV, corresponding to HOMO levels of –6.04, -6.06 and –6.14 eV. Similarly, the initial reduction potentials are -0.77, -0.80, and - 0.81 eV, and the LUMO levels of these emitters are -3.77, -3.98, and -3.50 eV.

Conclusion –

In summary, three novel TADF materials (***t*Cz-DibzPyrQx**, ***t*DPA-PyrQx**, and **Ac-DibzPyrQx**) were designed and synthesized using pyrazinoquinoxaline as a newly developed electron-accepting unit. These molecules possess color-tuning ability due to different donors, and pyrazinoquinoxaline as a robust acceptor region while allowing flexibility in the donor segment leading to twisted geometry necessary for small singlet-triplet energy gap (ΔE_{ST}). These emitter's shows broad absorption and emission spectra, also exhibit good thermal and electrochemical properties. So we stropngly believe that this work demonstrate great potential of the pyrazinoquinoxaline acceptor in developing highly efficient orange-red TADF emitters.

Acknowledgment –

SM has thankful to the Council of Scientific and Industrial Research [File No:09/0991(16403)/2023-EMR-I], New Delhi, India for providing a CSIR-JRF fellowship.

Reference –

1. Uoyama H, Goushi K, Shizu K, Nomura H, Adachi C. Highly efficient organic light-emitting diodes from delayed fluorescence. *Nature*. 2012;492(7428):234-238. doi:10.1038/nature11687
2. Wong MY, Zysman-Colman E. Purely Organic Thermally Activated Delayed Fluorescence Materials for Organic Light-Emitting Diodes. *Adv Mater*. 2017;29(22). doi:10.1002/adma.201605444
3. Yang Z, Mao Z, Xie Z, et al. Recent advances in organic thermally activated delayed

fluorescence materials. *Chem Soc Rev*. 2017;46(3):915-1016. doi:10.1039/c6cs00368k

4. Liu Y, Li C, Ren Z, Yan S, Bryce MR. All-organic thermally activated delayed fluorescence materials for organic light-emitting diodes. *Nat Rev Mater*. 2018;3. doi:10.1038/natrevmats.2018.20

5. Zhang D, Song X, Gillett AJ, et al. Efficient and Stable Deep-Blue Fluorescent Organic Light-Emitting Diodes Employing a Sensitizer with Fast Triplet Upconversion. *Adv Mater*. 2020;32(19):1-9. doi:10.1002/adma.201908355

6. Bunzmann N, Weissenseel S, Kudriashova L, et al. Optically and electrically excited intermediate electronic states in donor:acceptor based OLEDs. *Mater Horizons*. 2020;7(4):1126-1137. doi:10.1039/c9mh01475f

7. Tao Y, Yuan K, Chen T, et al. Thermally activated delayed fluorescence materials towards the breakthrough of organoelectronics. *Adv Mater*. 2014;26(47):7931-7958. doi:10.1002/adma.201402532

8. Uoyama H, Goushi K, Shizu K, Nomura H, Adachi C. Highly efficient organic light-emitting diodes from delayed fluorescence. *Nature*. 2012;492(7428):234-238. doi:10.1038/nature11687

9. Hong G, Gan X, Leonhardt C, et al. A Brief History of OLEDs—Emitter Development and Industry Milestones. *Adv Mater*. 2021;33(9). doi:10.1002/adma.202005630

10. Chen JX, Wang K, Xiao YF, et al. Thermally Activated Delayed Fluorescence Warm White Organic Light Emitting Devices with External Quantum Efficiencies Over 30%. *Adv Funct Mater*. 2021;31(31):1-8. doi:10.1002/adfm.202101647

11. Lee HL, Jeon SO, Kim I, et al. Multiple-Resonance Extension and Spin-Vibronic-Coupling-Based Narrowband Blue Organic Fluorescence Emitters with Over 30% Quantum Efficiency. *Adv Mater*. 2022;34(33):1-8. doi:10.1002/adma.202202464

12. Liu F, Cheng Z, Jiang Y, et al. Highly Efficient Asymmetric Multiple Resonance Thermally Activated Delayed Fluorescence Emitter with EQE of 32.8 % and Extremely Low Efficiency Roll-Off. *Angew Chemie - Int Ed*. 2022;61(14). doi:10.1002/anie.202116927

13. Lee YT, Chan CY, Tanaka M, et al. Investigating HOMO Energy Levels of Terminal Emitters for Realizing High-Brightness and Stable TADF-Assisted Fluorescence Organic Light-Emitting Diodes. *Adv Electron Mater*. 2021;7(4):1-9. doi:10.1002/aelm.202001090

14. Braveenth R, Lee H, Park JD, et al. Achieving Narrow FWHM and High EQE Over 38% in Blue OLEDs Using Rigid Heteroatom-Based Deep Blue TADF Sensitized Host. *Adv Funct Mater*. 2021;31(47). doi:10.1002/adfm.202105805

15. Lim H, Cheon HJ, Woo SJ, Kwon SK, Kim YH, Kim JJ. Highly Efficient Deep-Blue OLEDs using a TADF Emitter with a Narrow Emission Spectrum and High Horizontal Emitting Dipole Ratio. *Adv Mater*. 2020;32(47):1-8. doi:10.1002/adma.202004083

16. Huang T, Wang Q, Xiao S, et al. Simultaneously Enhanced Reverse Intersystem Crossing and Radiative Decay in Thermally Activated Delayed Fluorophors with Multiple Through-space Charge Transfers. *Angew Chemie - Int Ed*. 2021;60(44):23771-23776.

doi:10.1002/anie.202109041

17. Kaji H, Suzuki H, Fukushima T, et al. Purely organic electroluminescent material realizing 100% conversion from electricity to light. *Nat Commun*. 2015;6(May):2-9. doi:10.1038/ncomms9476

18. Sun JW, Lee JH, Moon CK, Kim KH, Shin H, Kim JJ. A fluorescent organic light-emitting diode with 30% external quantum efficiency. *Adv Mater*. 2014;26(32):5684-5688. doi:10.1002/adma.201401407

19. Uoyama H, Goushi K, Shizu K, Nomura H, Adachi C. Highly efficient organic light-emitting diodes from delayed fluorescence. *Nat 2012 4927428*. 2012;492(7428):234-238. doi:10.1038/nature11687

20. Wong SK tsung, Adachi C. As featured in : ChemComm Electroluminescence based on thermally activated delayed fluorescence. 2012;(207890):9580-9583. doi:10.1039/c2cc31468a

21. Wu CC, Lin CL, Cho TY, Yang CJ, Lu YJ. Electromagnetic modeling of OLEDs and its applications to advanced OLEDs. *J Inf Disp*. 2006;7(4):5-8. doi:10.1080/15980316.2006.9652012

22. Sun Y, Forrest SR, Sun Y. Organic light emitting devices with enhanced outcoupling via microlenses fabricated by imprint lithography Organic light emitting devices with enhanced outcoupling via microlenses. 2011;073106(2006):1-7. doi:10.1063/1.2356904

23. Chang HW, Lee J, Hofmann S, et al. Nano-particle based scattering layers for optical efficiency enhancement of organic light-emitting diodes and organic solar cells. *J Appl Phys*. 2013;113(20). doi:10.1063/1.4807000

24. Do YR, Kim YC, Song YW, et al. Enhanced light extraction from organic light-emitting diodes with 2D SiO2/SiNx photonic crystals. *Adv Mater*. 2003;15(14):1214-1218. doi:10.1002/adma.200304857

25. Feng J, Okamoto T, Kawata S. Highly directional emission via coupled surface-plasmon tunneling from electroluminescence in organic light-emitting devices. *Appl Phys Lett*. 2005;87(24):1-3. doi:10.1063/1.2142085

26. Cai X, Li X, Xie G, et al. "rate-limited effect" of reverse intersystem crossing process: The key for tuning thermally activated delayed fluorescence lifetime and efficiency roll-off of organic light emitting diodes. *Chem Sci*. 2016;7(7):4264-4275. doi:10.1039/c6sc00542j

27. Wang H, Zhao B, Qu C, et al. 2,3-Dicyanopyrazino phenanthroline enhanced charge transfer for efficient near-infrared thermally activated delayed fluorescent diodes. *Chem Eng J*. 2022;436(January):135080. doi:10.1016/j.cej.2022.135080

28. Wang S, Miao Y, Yan X, Ye K, Wang Y. A dibenzo[a, c] phenazine-11,12-dicarbonitrile (DBPzDCN) acceptor based thermally activated delayed fluorescent compound for efficient near-infrared electroluminescent devices. *J Mater Chem C*. 2018;6(25):6698-6704. doi:10.1039/c8tc01746h

29. Wang H, Zhou L, Shi YZ, et al. A facile strategy for enhancing reverse intersystem crossing

of red thermally activated delayed fluorescence emitters. *Chem Eng J*. 2022;433(P1):134423. doi:10.1016/j.cej.2021.134423

30. Xie F ming, Wu P, Zou S jie, et al. Efficient Orange – Red Delayed Fluorescence Organic Light-Emitting Diodes with External Quantum Efficiency over 26 %. 2020;1900843:1-7. doi:10.1002/aelm.201900843

31. Huang FX, Li HZ, Xie FM, et al. Efficient orange-red thermally activated delayed fluorescence material containing a cyano group. *Dye Pigment*. 2021;195(August):109731. doi:10.1016/j.dyepig.2021.109731

32. Wang H, Chen JX, Zhou L, et al. A dual-locked triarylamine donor enables high-performance deep-red/NIR thermally activated delayed fluorescence organic light-emitting diodes. *Mater Horizons*. Published online 2023. doi:10.1039/d3mh00445g

33. Yu L, Wu Z, Xie G, et al. Achieving a balance between small singlet-triplet energy splitting and high fluorescence radiative rate in a quinoxaline-based orange-red thermally activated delayed fluorescence emitter. *Chem Commun*. 2016;52(73):11012-11015. doi:10.1039/c6cc05203g

34. Li C, Duan R, Liang B, et al. Deep-Red to Near-Infrared Thermally Activated Delayed Fluorescence in Organic Solid Films and Electroluminescent Devices. *Angew Chemie - Int Ed*. 2017;56(38):11525-11529. doi:10.1002/anie.201706464

35. Ma B, Ding Z, Liu D, et al. A Feasible Strategy for a Highly Efficient Thermally Activated Delayed Fluorescence Emitter Over 900 nm Based on Phenalenone Derivatives. *Chem - A Eur J*. Published online 2023. doi:10.1002/chem.202301197

36. Congrave DG, Drummond BH, Conaghan PJ, et al. A Simple Molecular Design Strategy for Delayed Fluorescence toward 1000 nm. *J Am Chem Soc*. 2019;141(46):18390-18394. doi:10.1021/jacs.9b09323

37. Yang T, Liang J, Cui Y, et al. Achieving 34.3% External Quantum Efficiency for Red Thermally Activated Delayed Fluorescence Organic Light-Emitting Diode by Molecular Isomer Engineering. *Adv Opt Mater*. 2023;11(1):1-9. doi:10.1002/adom.202201191

38. Wang X, Zhou Y, Lei T, Hu N, Chen E qiang, Pei J. Structural - Property Relationship in Pyrazino [2 , 3-g] quinoxaline Derivatives : Morphology , Photophysical , and Waveguide Properties. 2010;(6):3735-3745. doi:10.1021/cm100798q

39. Chem JM, Tam TL, Zhou F, et al. Journal of Materials Chemistry. Published online 2011:17798-17804. doi:10.1039/c1jm12347e

40. Li H, Zhou F, Dexter L, Lam M, Mhaisalkar SG, Grimsdale AC. Journal of Materials Chemistry C. Published online 2013. doi:10.1039/c2tc00212d

41. Kose E, Tarkuc S, Baran D, Tanyeli C, Toppare L. Synthesis of new donor – acceptor polymers containing thiadiazoloquinoxaline and pyrazinoquinoxaline moieties : low-band gap , high optical contrast , and almost black colored materials. *Tetrahedron Lett*. 2011;52(21):2725-2729. doi:10.1016/j.tetlet.2011.03.078

42. Zhang LP, Li X, Liu T, Kang L, Huang X, Zhao Y. A water-soluble pyrazino[2,3-: G]

quinoxaline photosensitizer for high-efficiency one- And two-photon excited bioimaging and photodynamic therapy. *Chem Commun*. 2020;56(41):5544-5547. doi:10.1039/d0cc02285c

43. Swayamprabha SS, Jou J huei, Pal SK. Room-Temperature Columnar Liquid Crystalline Materials Based on Pyrazino[2,3-g]quinoxaline for Bright Green Organic Light-Emitting Diodes. *ACS Appl Electron Mater*. 2019;1:1959-1969. doi:10.1021/acsaelm.9b00477

44. Vishwakarma VK, Nagar MR, Lhouvum N, Jou J huei, Sudhakar AA. A New Class of Solution Processable Pyrazino [2 , 3-g] quinoxaline Carbazole Derivative Based on D – A – D Architecture for Achieving High EQE in Yellow and White OLEDs. 2022;2200241:1-14. doi:10.1002/adom.202200241

45. Yu L, Wu Z, Xie G, Zeng W, Ma D, Yang C. Molecular design to regulate the photophysical properties of multifunctional TADF emitters towards high-performance TADF-based OLEDs with EQEs up to 22.4% and small efficiency roll-offs. *Chem Sci*. 2018;9(5):1385-1391. doi:10.1039/c7sc04669c

46. Chen JX, Tao WW, Chen WC, et al. Red/Near-Infrared Thermally Activated Delayed Fluorescence OLEDs with Near 100 % Internal Quantum Efficiency. *Angew Chemie - Int Ed*. 2019;58(41):14660-14665. doi:10.1002/anie.201906575

47. Liang J, Li C, Cui Y, Li Z, Wang J, Wang Y. Rational design of efficient orange-red to red thermally activated delayed fluorescence emitters for OLEDs with external quantum efficiency of up to 26.0% and reduced efficiency roll-off. *J Mater Chem C*. 2020;8(5):1614-1622. doi:10.1039/c9tc05892c

48. Huang T, Liu D, Jiang J, Jiang W. Quinoxaline and Pyrido[x,y-b]pyrazine-Based Emitters: Tuning Normal Fluorescence to Thermally Activated Delayed Fluorescence and Emitting Color over the Entire Visible-Light Range. *Chem - A Eur J*. 2019;25(46):10926-10937. doi:10.1002/chem.201902116

49. Yu L, Wu Z, Xie G. Pyrido[2,3-b]pyrazine-based full-color fluoresent materials for high-performance OLEDs. Published online 2020:12445-12449. doi:10.1039/D0TC02412K

50. Zeng W, Zhou T, Ning W, et al. Realizing 22.5% External Quantum Efficiency for Solution-Processed Thermally Activated Delayed-Fluorescence OLEDs with Red Emission at 622 nm via a Synergistic Strategy of Molecular Engineering and Host Selection. *Adv Mater*. 2019;31(33):1-8. doi:10.1002/adma.201901404

51. Xie FM, Li HZ, Dai GL, et al. Rational Molecular Design of Dibenzo[a, c]phenazine-Based Thermally Activated Delayed Fluorescence Emitters for Orange-Red OLEDs with EQE up to 22.0%. *ACS Appl Mater Interfaces*. 2019;11(29):26144-26151. doi:10.1021/acsami.9b06401

Supporting Information

Materials and Methods

All reagents for the synthesis of Ac-DibzPyrQx and *t*Cz-DibzPyrQx were purchased from Sigma Aldrich, BLD pharma. ^{1}H NMR and ^{13}NMR measured on an Agilent 500MHz spectrometer. UV-visible and Photoluminescence are recorded with the Shimadzu UV 1800 spectrophotometer from 200 to 600 nm and Shimadzu RF 6000 spetrofluorophotometer in the range of 450 to 800 respectively having 10^{-5} mol/L concentration. Thermogravimetric analysis was undertaken with HITACHI STA7300 under a nitrogen atmosphere and heating at a rate of 10^{0}C/min from up to 600^{0}C. Electrochemical analysis was performed on a Metrohm Autolab PGSTAT204 Potentiostat/Galvanostat operating in cyclic voltammetry mode. Glassy carbon, Pt wire, and Ag/AgCl were employed as working, counter, and reference electrodes respectively. Tetrabutyl ammonium perchlorate (0.1 mol/L) was dissolved in DMF and Tetrabutylammonium hexafluorophosphate was dissolved in DCM (0.1 mol/L) used as an electrolytes and the scan rate was 100mV/sec.

Experimental

Synthesis of 1-(4-(3,6-di-tert-butyl-9H-carbazol-9-yl)phenyl)-2-phenylethane-1,2-dione

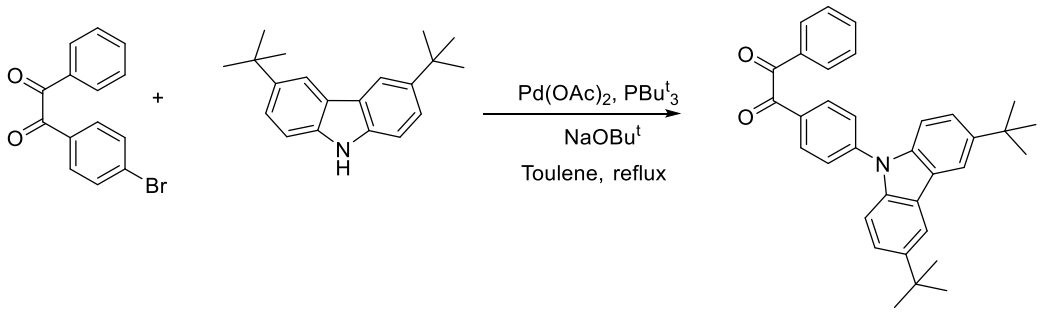

A mixture of 1-(4-bromophenyl)-2-phenylethane-1,2-dione (5.0 g, 1.73mmol) and 3,6-di-*tert*-butyl-9H-carbazole (0.47 g, 1.73 mmol) and K_2CO_3 (0.7 g, 3.00 mmol) were added into three neck flask in 50 ml toluene in N_2 atmosphere. After degassing for 15 min, $Pd(OAc)_2$ (10 mol%) and tri-*tert*-butylphosphine (0.146 ml, 0.62 mmol) were added. Subsequently, the mixture was stirred and refluxed overnight. After removing the solvent in vacuum, the mixture was partitioned between

DCM and water. The combined organic layers were washed with brine, dried over Mg_2SO_4 and concentrated in vacuum. Column chromatography of the residue solid. (0.71g, 84%)

Synthesis of 1-(4-(bis(4-(*tert*-butyl)phenyl)amino)phenyl)-2-phenylethane-1,2-dione

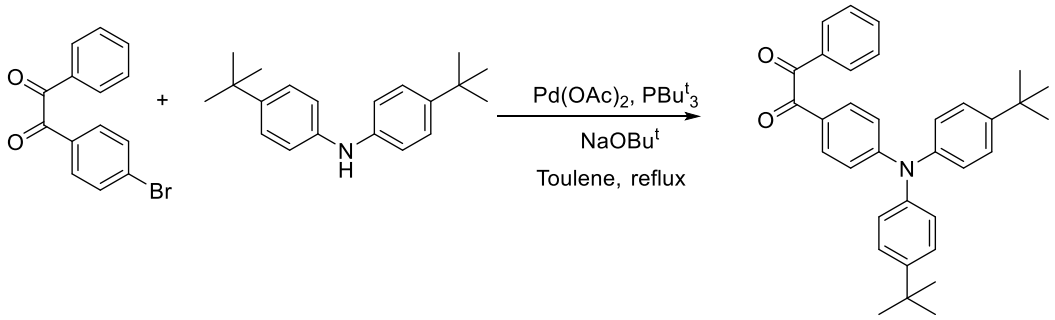

A mixture of 1-(4-bromophenyl)-2-phenylethane-1,2-dione (5.0 g, 1.73mmol) and bis(4-(*tert*-butyl)phenyl)amine (0.46 g, 1.73 mmol) and K_2CO_3 (0.7 g, 3 mmol) were added into three neck flask in 50 ml toluene in N_2 atmosphere. After degassing for 15 min, $Pd(OAc)_2$ (10 mmol%) and tri-tert-butylphosphine (0.146 ml, 0.62 mmol) were added. Subsequently, the mixture was stirred and refluxed overnight. After removing the solvent in vacuum, the mixture was partitioned between DCM and water. The combined organic layers were washed with brine, dried over Mg_2SO_4 and concentrated in vacuum. Column chromatography of the residue solid. (0.72 g, 85%).

Synthesis of 1-(4-(9,9-dimethylacridin-10(9H)-yl)phenyl)-2-phenylethane-1,2-dione

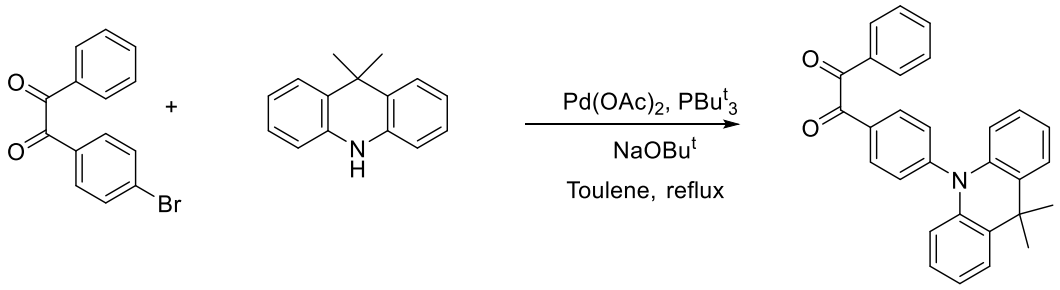

A mixture of 1-(4-bromophenyl)-2-phenylethane-1,2-dione (5.0 g, 1.73 mmol) and 9,9-dimethyl-9,10-dihydroacridine, (0.36g, 1.73mmol) and K_2CO_3 (0.7 g, 3 mmol) were added into three neck flask in 50 ml toluene in N2 atmosphere. After degassing for 15min, $Pd(OAc)_2$ (10 mol%) and tri-*tert*-butylphosphine (0.146 ml, 0.62 mmol) were added. Subsequently, the mixture was stirred and refluxed overnight. After removing the solvent in vacuum, the mixture was partitioned between DCM and water. The combined organic layers were washed with brine, dried over Mg_2SO_4 and concentrated in vacuum. Column chromatography of the residue solid. (0.63 g, 87%)

Synthesis of 2,3-diphenyl quinoxaline-6,7-diamine (I)

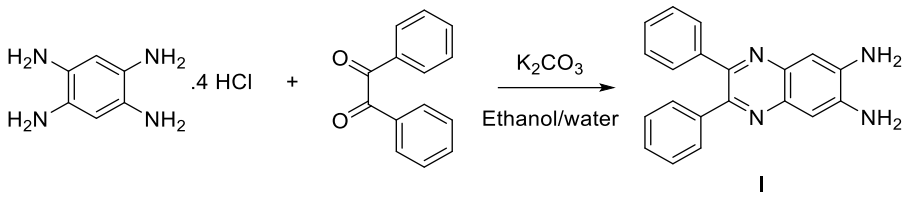

I

1,2,4,5-Benzenetetramine tetrahydrochloride (0.5 g, 3.62mmol) is dissolved in ethanol then K_2CO_3 (1.0 g, 7.24 mmol) is added to the reaction mixture then Benzil (0.76g, 3.62mmol) is added slowly then the reaction was refluxed 8 hr. After cooling to room temperature water was added and extracted with ethyl acetate. Then it is purified by using column chromatography. (0.42 g, 37.16%).

Synthesis of 2-(4-(3,6-di-tert-butyl-9H-carbazol-9-yl)phenyl)-3,7,8-triphenylpyrazino[2,3-g]quinoxaline (*t*Cz-PyrQx)

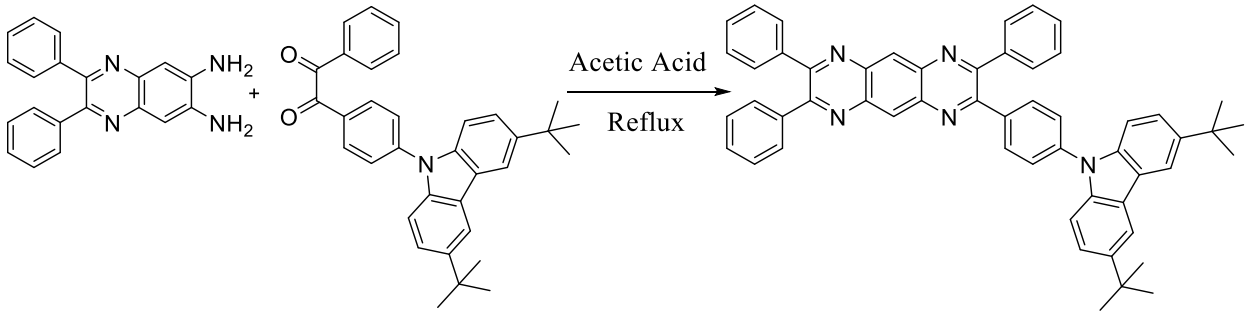

Intermediate I (0.8 g, 2.56 mmol) and 1-(4-(3,6-di-tert-butyl-9H-carbazol-9-yl)phenyl)-2-phenylethane-1,2-dione (1.25 g, 2.56 mmol) were dissolved in acetic acid and the mixture was heated to reflux for 12 hrs. The reaction mixture was cooled to room temperature and water was added. The yellow solid precipitated out was filtered and purified by column chromatography. (1.48g, 76.28%). ^{1}H NMR (500 MHz, $CDCl_3$) δ 9.08 (s, 1H), 9.07 (s, 1H), 8.14 (d, *J* = 1.7 Hz, 2H), 7.85 (d, *J* = 1.7 Hz, 1H), 7.83 (d, *J* = 1.7 Hz, 1H), 7.72 (dd, *J* = 7.8, 1.5 Hz, 2H), 7.64 (d, *J* = 1.1 Hz, 2H), 7.63 – 7.59 (m, 5H), 7.51 – 7.46 (m, 5H), 7.45-7.42 (m, 5H), 7.41 (d, *J* = 2.8 Hz, 2H), 1.48 (s, , 18H).

Synthesis of 4-(tert-butyl)-N-(4-(tert-butyl)phenyl)-N-(4-(3,7,8-triphenylpyrazino[2,3-g]quinoxalin-2-yl)phenyl)aniline (*t*DPA-PyrQx)

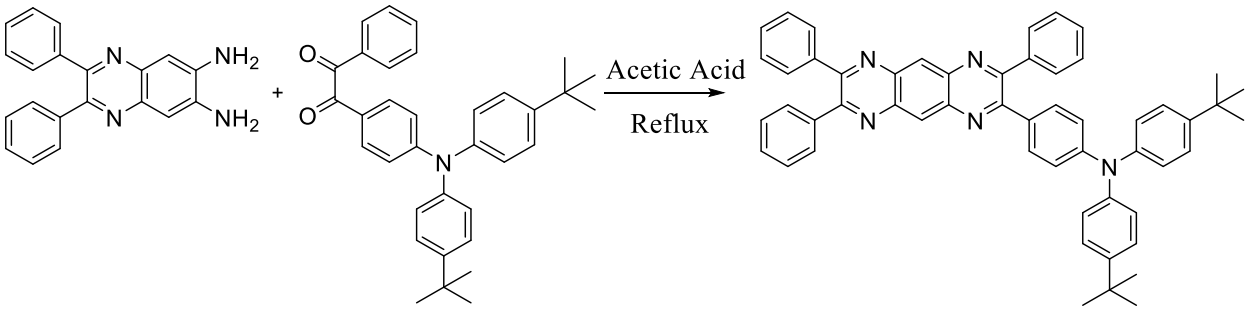

Intermediate I (0.8 g, 2.56mmol) and 1-(4-(bis(4-(*tert*-butyl)phenyl)amino)phenyl)-2-phenylethane-1,2-dione (1.25 g, 2.56 mmol) were dissolved in acetic acid and the mixture was heated to reflux for 12 hrs. The reaction mixture was cooled to room temperature and water was added. The red solid precipitated out was filtered and purified by column chromatography. (1.5 g, 76.53%). ^{1}H NMR (500 MHz, $CDCl_3$) δ 8.97 (s, 1H), 8.96 (s, 1H), 7.70 (d, *J* = 7.2 Hz, 2H), 7.61 (d, *J* = 7.2 Hz, 5H), 7.44 (d, *J* = 6.8 Hz, 4H), 7.39 (dt, *J* = 14.0, 7.0 Hz, 5H), 7.29 (d, *J* = 8.4 Hz, 4H), 7.07 (d, *J* = 8.4 Hz, 5H), 6.97 (d, *J* = 8.5 Hz, 2H), 1.32 (s, 18H).

Synthesis of 2-(4-(9,9-dimethylacridin-10(9H)-yl)phenyl)-3,7,8-triphenylpyrazino[2,3-g]quinoxaline. (Ac-PyrQx)

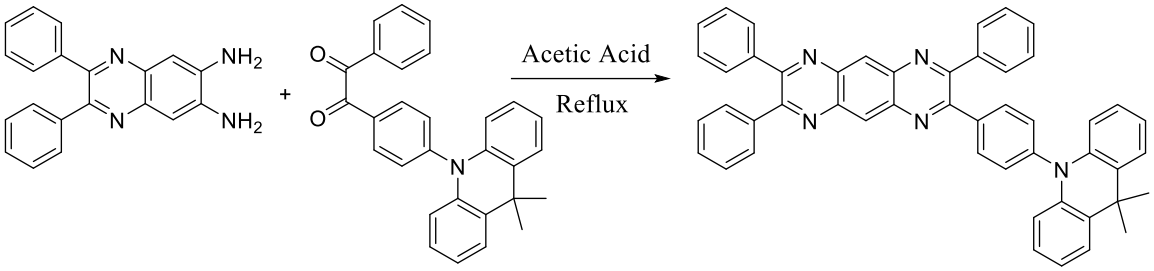

Intermediate I (0.8 g, 2.56 mmol) and 1-(4-(9,9-dimethylacridin-10(9H)-yl)phenyl)-2-phenylethane-1,2-dione (1.0 g, 2.56 mmol) were dissolved in acetic acid and the mixture was heated to reflux for 12 hrs. The reaction mixture was cooled to room temperature and water was added. The yellow solid precipitated out was filtered and purified by column chromatography. (1.32 g, 74.57%) ^{1}H NMR (500 MHz, $CDCl_3$) δ 9.09 (s, 1H), 9.08 (s, 1H), 7.85 (d, *J* = 8.4 Hz, 2H), 7.69 (dd, *J* = 7.8, 1.7 Hz, 2H), 7.65 (t, *J* = 1.1 Hz, 2H), 7.64 – 7.63 (m, 2H), 7.47 (dd, *J* = 7.7, 1.5 Hz, 2H), 7.45 (t, *J* = 2.0 Hz, 2H), 7.44 – 7.42 (m, 2H), 7.41 (d, *J* = 1.3 Hz, 1H), 7.40 (d, *J* = 1.7 Hz, 2H), 7.38 (t, *J* = 2.0 Hz, 2H), 7.37 (d, *J* = 1.9 Hz, 1H), 6.99 (dtd, *J* = 30.3, 7.3, 1.4 Hz, 5H), 6.35 (dd, *J* = 8.1, 1.2 Hz, 2H), 1.69 (d, *J* = 5.7 Hz, 6H).

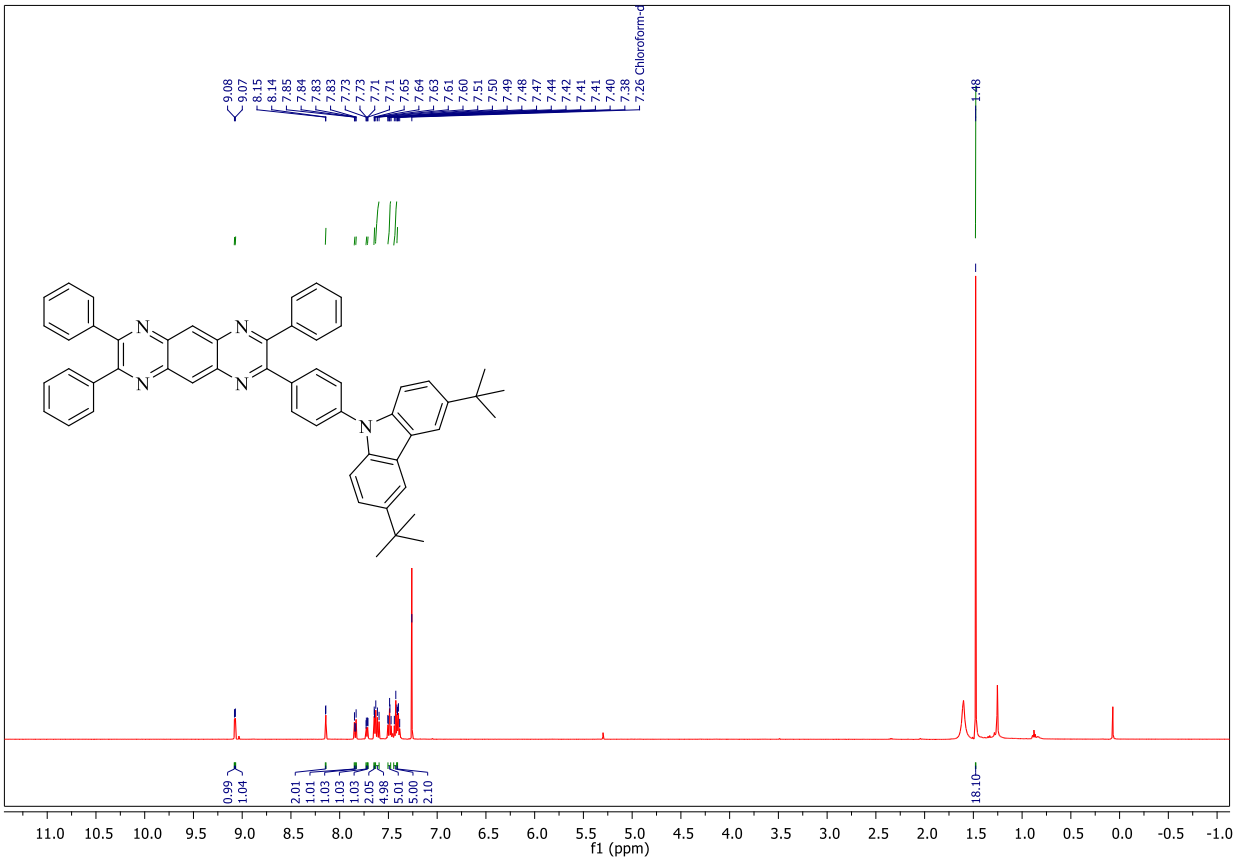

Fig. S1 ^{1}H spectra of ^{t}Cz-PyrQx

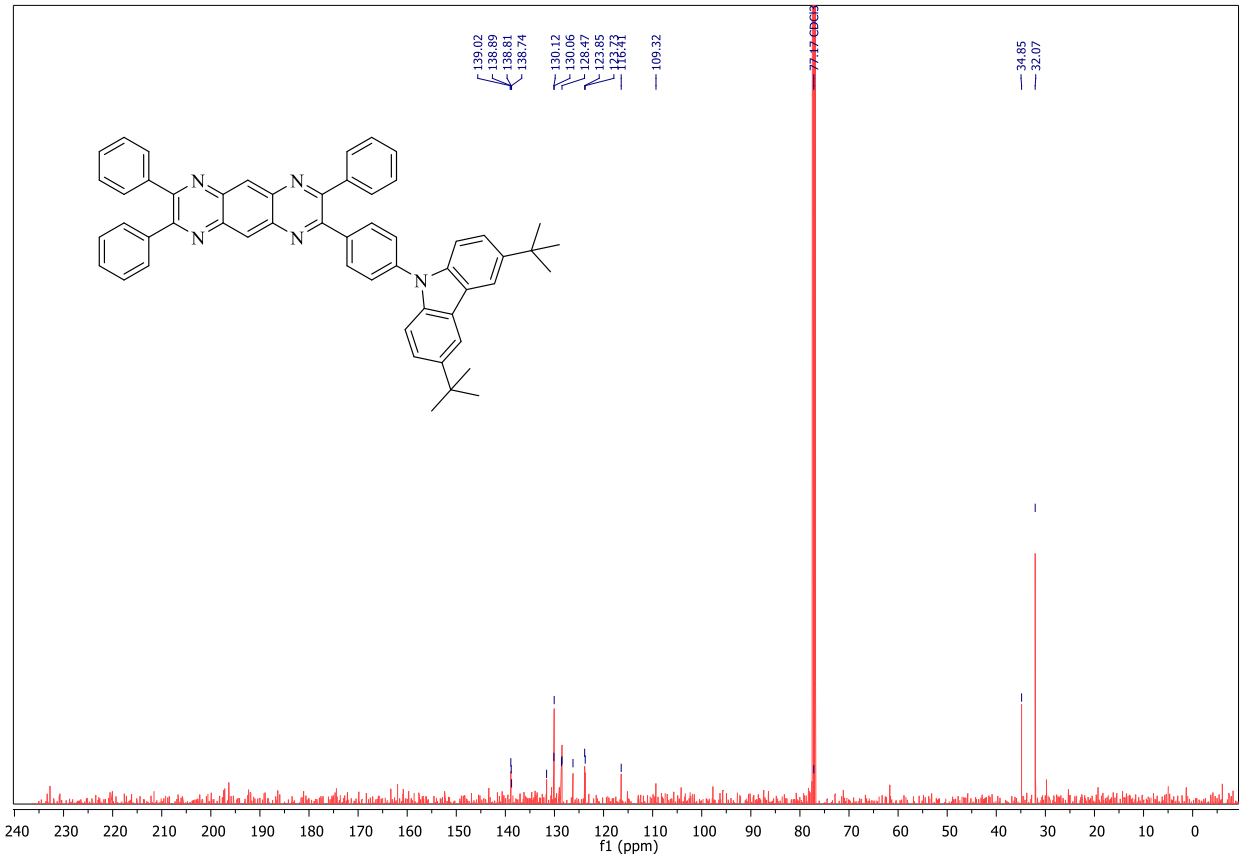

Fig. S2 ^{13}C spectra of ^{t}Cz-PyrQx

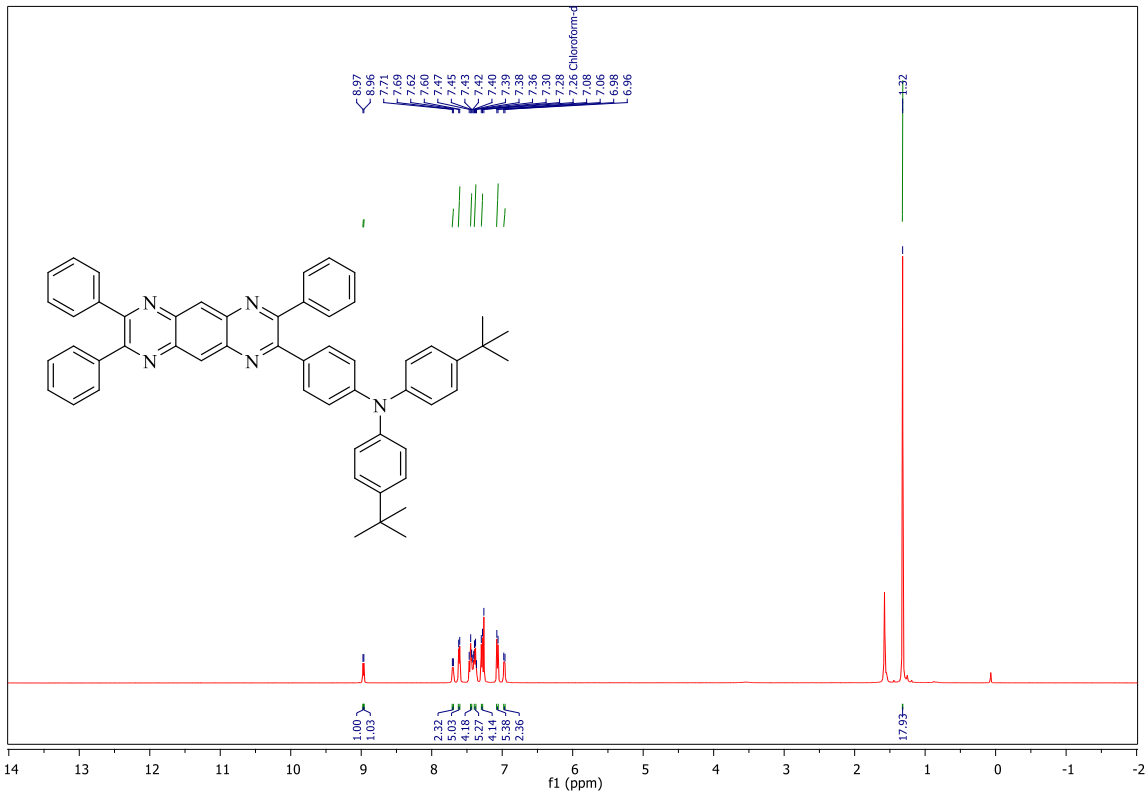

Fig. S3 ^{1}H spectra of ^{t}DPA-PyrQx

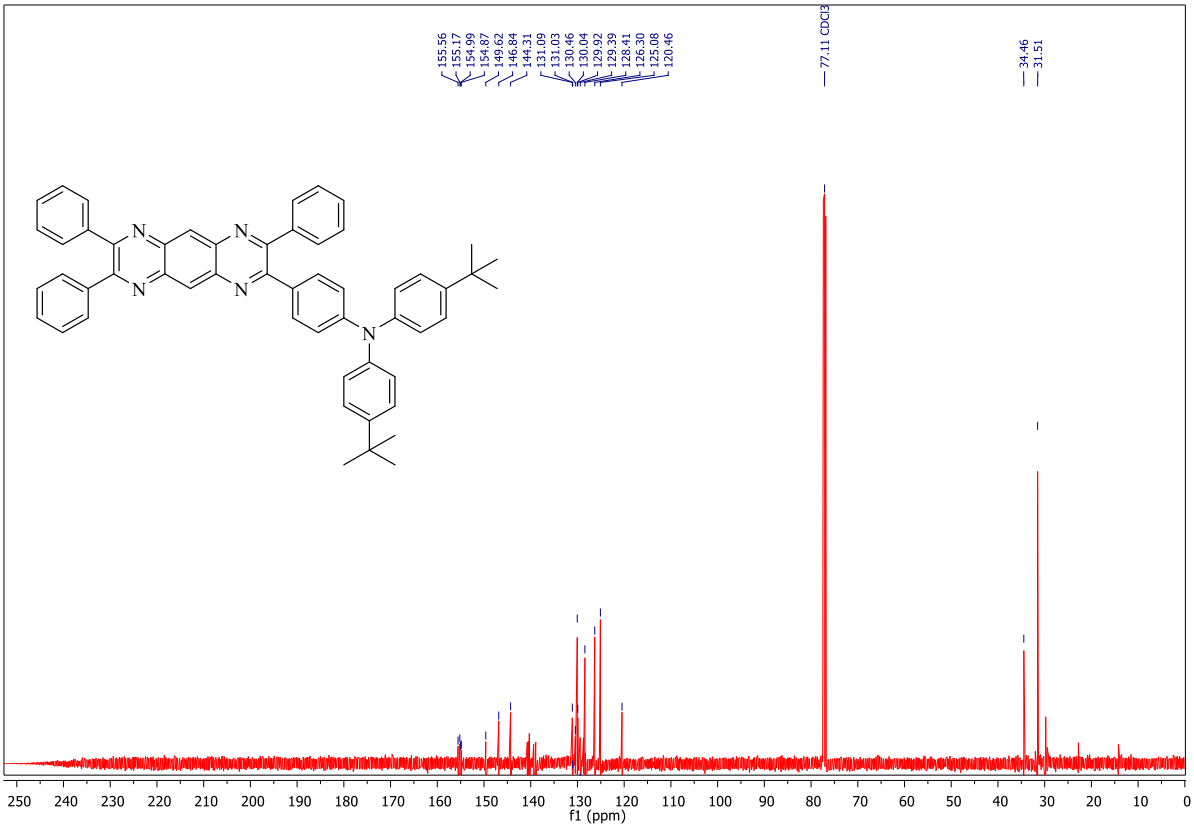

Fig. S4 ^{13}C spectra of ^{t}DPA-PyrQx

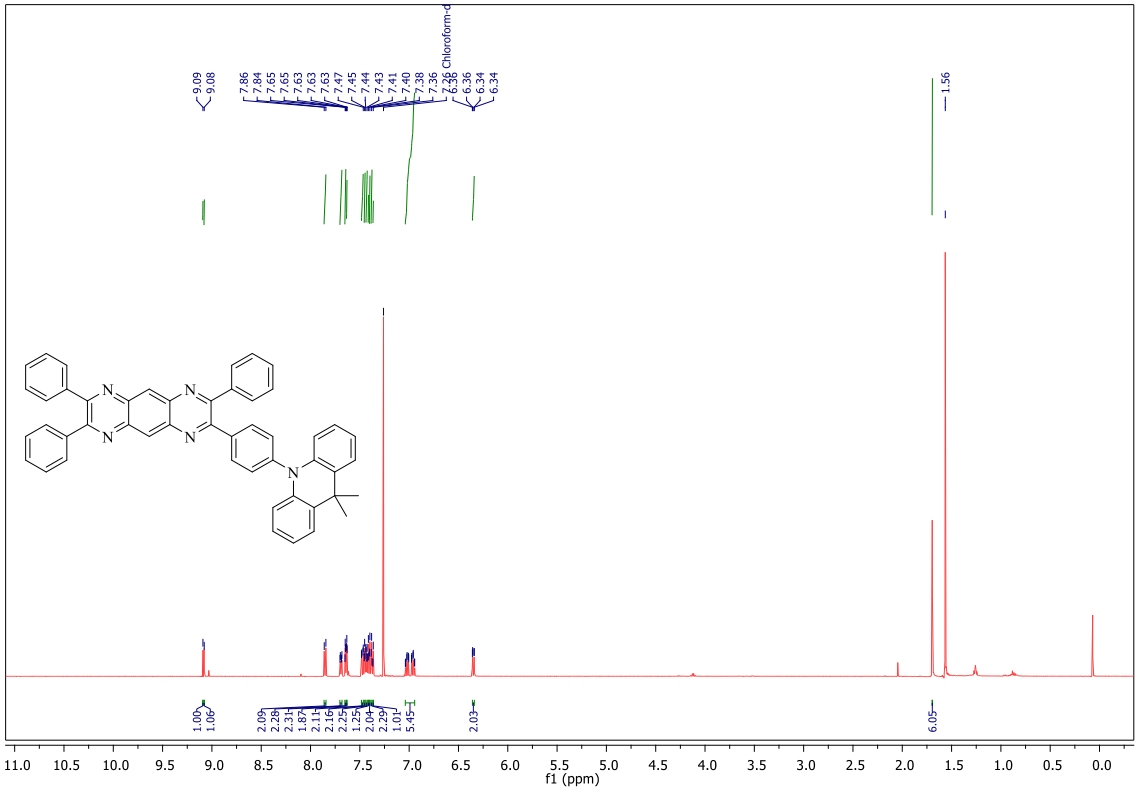

Fig. S5 ^{1}H spectra of Ac-PyrQx

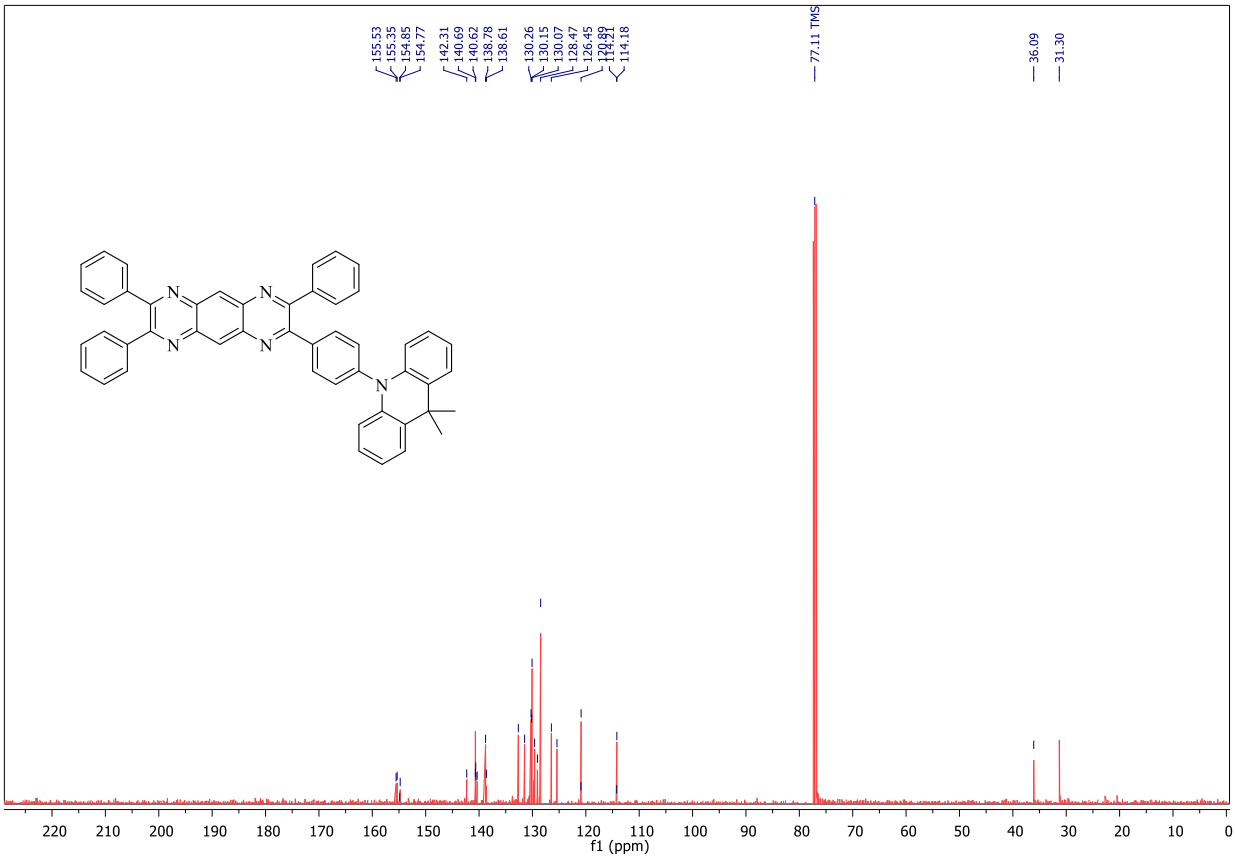

Fig. S6 ^{13}C spectra of Ac-PyrQx